Brillouin scattering in $KTiOPO_4$, $RbTiOPO_4$ and $TlTiOPO_4$: a study of the ferroelectric-paraelectric phase transition

1994 J. Phys.: Condens. Matter 6 3821

(http://iopscience.iop.org/0953-8984/6/20/022)

J. Phys.: Condens. Matter 6 (1994) 3821–3830. Printed in the UK

Brillouin scattering in $KTiOPO_4$, $RbTiOPO_4$ and $TlTiOPO_4$: a study of the ferroelectric–paraelectric phase transition

M Serhane and P Moch

Laboratoire des Propriétés Mécaniques et Thermodynamiques des Matériaux, CNRS, Université Paris-Nord, 93430, Villetaneuse, France

Received 6 December 1993, in final form 25 January 1994

Abstract. Brillouin scattering measurements have been performed on isostructural ferroelectric crystals $KTiOPO_4$ (KTP), $RbTiOPO_4$ (RTP) and $TlTiOPO_4$ (TTP) as functions of the temperature. At room temperature, all the elastic constants have been determined. The temperature variations in the longitudinal elastic constants (for TTP and RTP) reveal similar behaviours; they agree with a Landau model for a second-order phase transition where the order parameter is quadratically coupled to the strains. An intense quasi-elastic light scattering signal, related to the ionic conductivity, is observed in the spectra. In addition, a central peak apparently connected with the locking of the soft mode is observed for RTP near its phase transition.

1. Introduction

Potassium titanyl phosphate $KTiOPO_4$ (KTP) is exceptional in its overall properties which are very close to matching all the requirements for a material well suited to second-harmonic generation. Many chemical modifications of KTP have already been synthesized; among them, rubidium titanyl phosphate $RbTiOPO_4$ (RTP) and thallium titanyl phosphate $TlTiOPO_4$ (TTP), which are obtained by cationic substitution, show similar properties.

At room temperature, the crystal symmetry of these ferroelectric (FE) isostructural compounds is orthorhombic, the polar space group being $Pna2_1$ (C_{2v}^9) [1]. The primitive unit cell contains eight formula units. The crystal framework is constructed with chains of TiO_6 octahedra linked by PO_4 tetrahedra. Such structural elements (TiO_6 or PO_4) are also found in other FEs (perovskite-type $ATiO_3$ and KH_2PO_4). The TiO_6 octahedra are highly distorted and contain anomalously short Ti–O bonds associated with the non-linear optical properties of these compounds [2, 3]. This framework shows channels parallel to the c polar axis, through which K, Rb or Tl ions can easily move under the influence of an electric field. The ionic conductivity is quasi one dimensional; along the c polar axis it is higher by four orders of magnitude than perpendicular to it [4, 5].

Furthermore, KTP, RTP and TTP undergo a structural phase transition (PT) from the low-temperature FE phase to a high-temperature paraelectric (PE) phase at temperatures T_c of 1206 K [6], 1040 K [7] and 885 K [6], respectively. The crystal structure of TTP has been studied at 923 K by neutron scattering [8]; this shows that the PE phase belongs to the centrosymmetric space group $Pnan$ (D_{2h}^6). Thomas *et al* [9] have suggested a model for the PE phase in KTP involving the same space group. The PE–FE phase transition has been experimentally studied by various techniques including second-harmonic generation [6], dielectric [6, 10], refringence [7], birefringence [11] and Raman scattering measurements [12]. These measurements demonstrate continuous changes in the physical quantities at

0953-8984/94/203821+10$19.50

T_c, suggesting that the transition is displacive and of second-order type. Pisarev *et al* [12] reported that the cation and the TiO_6 octahedron both play a significant role in the PT. For TTP a soft mode related to the Tl^+ motion has been observed in the FE phase; its temperature variation satisfactorily agrees with a classical second-order transition described by a Landau model. For RTP and KTP, soft modes are also observed, but with complicated behaviours versus temperature which suggest a coupling to a relaxation mode, giving rise to frequency locking [12–14].

For a better understanding of the mechanism of the PT we have studied the evolution of some elastic constants versus temperature by means of Brillouin scattering. Section 2 is devoted to the experimental procedures. In section 3.1 we present all the elastic constants of KTP, RTP and TTP at room temperature. Section 3.2.1 deals with the study of the variations in the longitudinal constants C_{ii} ($i = 1, 2, 3$) versus temperature which, in the case of RTP and TTP, are analysed using a phenomenological Landau model; for KTP, owing to the very high transition temperature T_c there is severe sample damage around T_c which precluded precise measurements of the C_{ii} variations near the PT. Finally, as described in section 3.2.2, the Brillouin spectra show additional features centred at zero frequency, partially due to ionic conductivity and partially arising from the above-mentioned mode coupling.

2. Experimental procedures

The KTP, RTP and TTP single crystals studied were grown in the Physics Department of Moscow University, using a flux method. At room temperature they show a good optical quality. They were cut as rectangular parallelipipeds with (100), (010) and (001) faces. The dimensions of the samples were approximately 2 mm × 2 mm × 2 mm. In the following, an orthogonal Cartesian coordinate system X, Y and Z is set with the X, Y, Z axes parallel to a, b and c, respectively. For the orthorhombic crystal classes, these axes coincide with the principal axes of the ellipsoid of indices.

At room temperature, 90° scattering and back-scattering polarized Brillouin spectra were recorded using a five-pass Fabry–Pérot interferometer and an argon ion laser working at 514.5 nm. For measurements versus temperature, we designed a furnace, allowing back-scattering experiments up to about 1200 K; the temperature was regulated to within about ±2 K; concerning its absolute value the uncertainty is rather large (10 K). As is well known, the Brillouin frequency shift is given by

$$\Delta\nu = \pm\frac{V_q}{\lambda}(n_i^2 + n_s^2 - 2n_i n_s \cos\theta)^{1/2} \tag{1}$$

where n_i and n_s are the refractive indices for the incident beam and the scattered beam, respectively, at $\lambda = 514.5$ nm, θ is the scattering angle and V_q is the velocity of the studied acoustic phonon propagating with the wavevector q.

As discussed above, the crystals studied show a high birefringence; it is shown that the frequency shifts significantly depend upon the polarizations of the incident light and of the scattered light. On the other hand, the direction of q and, consequently, the velocities also depend upon the indices involved; however, we have verified that, within the experimental accuracy, this last effect can be neglected. At room temperature the principal refractive indices are shown in table 1; for KTP and RTP they are taken from the work of Zumsteg *et al* [2]; for TTP, they were estimated by Aleksandrov *et al* [15] using the Chaulnes method, which unfortunately provides very inaccurate values. The values of the refractive indices

Table 1. Principal refractive indices at room temperature for $\lambda = 514.5$ nm.

Refractive index	Value for the following compounds		
	KTP [2]	RTP [2]	TTP [15]
n_1	1.79	1.82	2.08
n_2	1.80	1.84	2.13
n_3	1.91	1.93	2.18

versus temperature were estimated using the published data concerning their temperature variations [7].

In principle, in the FE phase, since the crystals belong to a polar class, the piezoelectric coefficients have to be taken into account in the equations of motion. The result is that [16]

$$\left(\rho V_q^2 \delta_{ik} - C^E_{ijkl}\hat{q}_j\hat{q}_l - \frac{(e_{j,li}\hat{q}_j\hat{q}_l)(e_{p,rk}\hat{q}_p\hat{q}_r)}{\varepsilon^s_{mn}\hat{q}_m\hat{q}_n}\right) u_i = 0 \tag{2}$$

where u_i stands for a component of the displacement, $\hat{q}$ is a unit vector parallel to the direction of propagation and ρ is the specific mass. In our analysis we did not take into account the temperature variation in ρ; from the previously published crystallographic data [7] it can be neglected within the experimental accuracy of the Brillouin measurements. In equation (2), C^E_{ijkl} is the elastic stiffness modulus at constant electric field, $e_{j,li}$ is the piezoelectric stress constant and ε^s_{mn} is the permittivity at constant strain. For KTP-type crystals, the non-vanishing C^E_{ijkl}, $e_{j,li}$ and ε^s_{mn} are, in Voigt notation, C^E_{11}, C^E_{22}, C^E_{33}, C^E_{44}, C^E_{55}, C^E_{66}, C^E_{12}, C^E_{13}, C^E_{23}, e_{15}, e_{24}, e_{31}, e_{32}, e_{33}, ε^s_{11}, ε^s_{22} and ε^s_{33}.

3. Results and discussion

The above-mentioned choice of the sample orientations allows one to study three different directions of the phonon wavevector using back-scattering measurements and three other directions using 90° measurements. Taking into account the selection rules for Brillouin scattering (table 2) [17], the back-scattering measurements allow observation of only longitudinal modes, while the 90° arrangement gives access to the three modes related to the geometrically imposed direction of the wavevector. Strictly speaking, this does not allow complete determination of the whole set of C^E_{ijkl} and $e_{j,li}$; of the stiffness constants, only C^E_{11}, C^E_{22}, C^E_{44}, C^E_{55}, C^E_{66} and C^E_{12} can be derived. As an example, table 2 shows the expressions for the velocities and the selection rules with light propagation in the (001) plane. However, as mentioned below, we experimentally found that, within the experimental accuracy, the piezoelectric correction can be neglected. The precision in back-scattering frequency measurements is better than 0.5% while in 90° experiments the uncertainty can reach a few per cent, owing to the geometrically induced line broadening and the lower scattered intensity.

3.1. Room-temperature measurements

Our analysis of the data has shown that, within the experimental accuracy, the piezoelectric contribution cannot be detected: it does not exceed about 2%, which means that $|e_{j,li}|$ is smaller than 0.4 C m^{-2} in the three crystals studied. In table 3, we give the stiffness constants for the three crystals at room temperature. Our results differ slightly from the

Table 2. Scattering geometries and the corresponding values of ρV_q^2 in the (001) plane obtained in the orthorhombic phase [17, 18]: L, longitudinal; T, transverse; QL, quasi-longitudinal; QT, quasi-transverse. When the piezoelectric terms can be neglected, the results for other geometries are obviously obtained through straightforward permutations. The expressions including the piezoelectric terms can also be derived easily.

Wavevector direction	Geometry	ρV_q^2	Mode
[100]	$X(YY)\bar{X}$ or $X(ZZ)\bar{X}$	C_{11}^E	L
[110]	$X(ZZ)Y$ or $X(YX)Y$	$\frac{1}{4}\{C_{11}^E + C_{22}^E + 2C_{66}^E + [(C_{11}^E - C_{22}^E)^2 + 4(C_{12}^E + C_{66}^E)^2]^{1/2}\}$	QL
		and	
		$\frac{1}{4}\{C_{11}^E + C_{22}^E + 2C_{66}^E - [(C_{11}^E - C_{22}^E)^2 + 4(C_{12}^E + C_{66}^E)^2]^{1/2}\}$	QT
[110]	$X(ZX)Y$ or $X(YZ)Y$	$\frac{1}{2}(C_{44}^E + C_{55}^E) + \frac{(e_{15} + e_{24})^2}{\varepsilon_1^s + \varepsilon_2^s}$	T
[010]	$Y(XX)\bar{Y}$ or $Y(ZZ)\bar{Y}$	C_{22}^E	L

previously published partial determinations [15], which, in our opinion, did not properly take the birefringence effects into account. For the 'longitudinal' C_{ii} $(i = 1, 2, 3)$, which were studied through back-scattering, the Brillouin frequency is written as

$$\Delta\nu_{ij} = \frac{2}{\rho^{1/2}\lambda^2} n_j (C_{ii})^{1/2} \qquad (j \neq i) \tag{3}$$

where λ is the illuminating wavelength and where j defines the common polarization of the incident and scattered light. In the case of KTP and RTP, the j-dependence fully agrees with the previously reported values of the refractive indices. We conclude that there is very good accuracy in the determination of the absolute values of C_{11} and C_{22} (concerning C_{33} the higher uncertainty could derive from the neglected piezoelectric term e_{33}^2/ε_3^s). In the case of TTP, the observed j-dependence allowed us to evaluate the ratios of the principal indices of refraction; they differ significantly from the previously published data. Unfortunately the Brillouin spectra allow the determination of only the different products $n_j(C_{ii})^{1/2}$ $(i \neq j;$ $i, j = 1, 2, 3)$; as a consequence, in table 3 the results concerning TTP arbitrarily state that $n_1 = 2.10$.

Table 3. Room-temperature values of the elastic constants for KTP, RTP and TTP. The values in parentheses indicate previously published results [15].

Elastic constant	Value (GPa) for the following compounds		
	KTP	RTP	TTP
C_{11}	166 (159 ± 3)	163 (143 ± 3)	156 (155 ± 5)
C_{22}	164 (154 ± 3)	165 (142 ± 3)	154 (154 ± 5)
C_{33}	181 (175 ± 3)	178 (175 ± 3)	166 (161 ± 5)
C_{44}	56	58 (33 ± 7)	45
C_{55}	54	57 (40 ± 8)	49
C_{66}	45	50 (57 ± 9)	49
C_{12}	37	45	40
C_{13}	54	35	49
C_{23}	51	70	63

The precision in the 'transverse' diagonal constants C_{ii} $(i = 4, 5, 6)$ is lower; it becomes significantly poorer for the non-diagonal C_{ij} $(i \neq j)$ which are evaluated in a rather indirect way, leading to an uncertainty which can rise to 15%.

However, from an overall comparative examination of the stiffness constants (table 3) in the three compounds, we conclude that, as expected, their elastic properties are very close.

3.2. Temperature dependence and phase transitions

3.2.1. Elastic constants. Owing to the above-mentioned uncertainties concerning the other stiffness constants, we have restricted our study to the 'longitudinal' elastic constants C_{11}, C_{22} and C_{33} determined by back-scattering measurements. The observed singularities around T_c (about 855 K for TTP and about 1035 K for RTP) are nearly identical for TTP and RTP. Figure 1 shows these frequency variations as functions of the temperature for TTP. The derived elastic constants for TTP and RTP deduced from equation (3) are plotted in figure 2; we took into account the temperature dependence of the refractive indices deduced from [7]. The elastic constant C_{22} does not show any anomaly at T_c. On the contrary, C_{11} and C_{33} reveal several interesting anomalies which agree with the previously reported hypothesis of a second-order displacive transition.

In order to discuss our results we make use of a phenomenological expression for the free-energy density F as a function of the temperature, of the order parameter η and of the strain components e_m:

$$F = F_\eta + F_c + F_m \tag{4}$$

$$F_\eta = \tfrac{1}{2}a(T - T_c)\eta^2 + b\eta^4 \qquad (a > 0, b > 0) \tag{5}$$

$$F_c(e_m, \eta) = \sum_{i=1}^{3} g_i e_i \eta^2 + \tfrac{1}{2}\sum_{i=1}^{6} h_i e_i^2 \eta^2 + \tfrac{1}{2}\sum_{1\leqslant i<j\leqslant 3} h_{ij} e_i e_j \eta^2 \tag{6}$$

$$F_m(e_m) = \tfrac{1}{2}\sum_{i=1}^{6} C_{ii}^0 e_i^2 + \sum_{1\leqslant i<j\leqslant 3} C_{ij}^0 e_i e_j. \tag{7}$$

The order parameter η is expected to be connected to the soft transverse mode observed in the ferroelectric phase [12] and belonging to the irreducible representation A_1. F_c describes the coupling of η to the strains; it can be shown by symmetry arguments that the coupling terms are even in the order parameter; we kept only the lowest-order terms, which are quadratic in η. A term such as $ge\eta^2$ leads to a typical step-like discontinuity. Anomalies of this type are observed in C_{11} only (figure 2(*a*)). A term such as $he^2\eta^2$ does not produce any discontinuity but provides singularities observed in C_{33} only (figure 2(*c*)). Thus, in the following discussion, we take $g_2 = g_3 = 0$ and $h_1 = h_2 = 0$. In addition, we take into account the thermal expansion of the prototype phase which introduces a linearly temperature-dependent term in C_{ii}^0:

$$C_{ii}^0(T) = C_{ii}^0(T_c)[1 + \delta_i(T_c - T)] \tag{8}$$

with $\delta_i > 0$. In the static approximation, if we neglect the fluctuations, C_{ii} can be written as [19]

$$C_{ii}(T) = \frac{\partial^2 F}{\partial \varepsilon_i^2} - \left(\frac{\partial^2 F}{\partial \eta \partial \varepsilon_i}\right)^2 \left(\frac{\partial^2 F}{\partial \eta^2}\right)^{-1}. \tag{9}$$

With these assumptions, the temperature dependences of the longitudinal elastic constants are easily derived. The resulting expressions are listed in table 4. Those related to

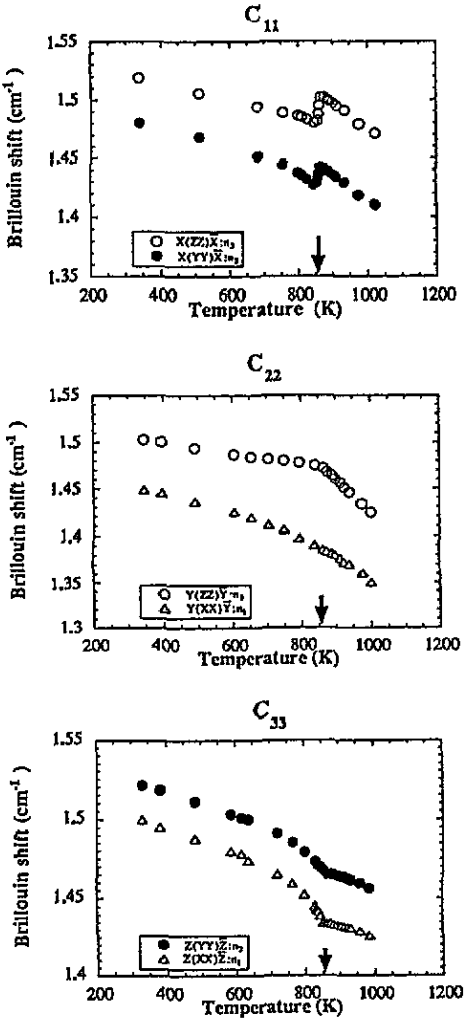

Figure 1. Temperature dependences of the Brillouin shifts of the longitudinal modes recorded with different back-scattering geometrical arrangements for TTP. The arrows indicate the transition temperatures.

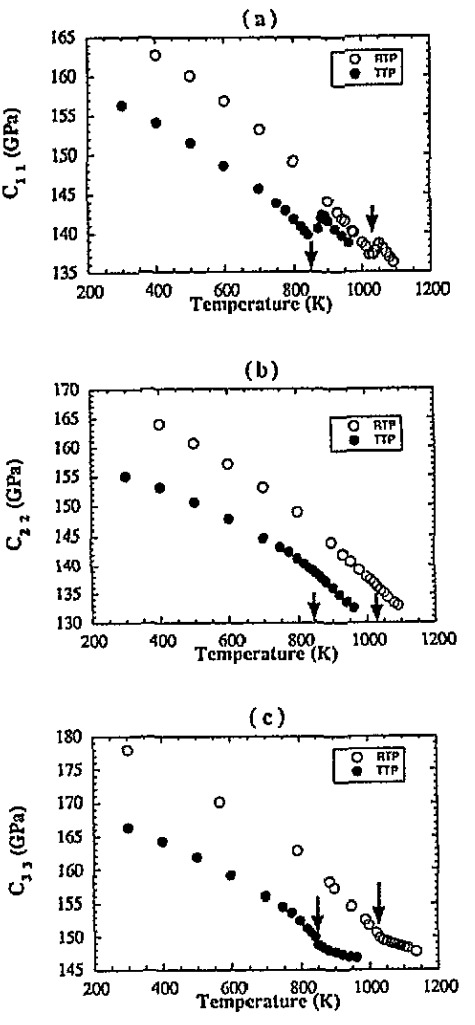

Figure 2. Variation in the longitudinal elastic constants for RTP and TTP versus temperature. The arrows indicate the transition temperatures.

the evolution of $C_{11}(T)$ and $C_{22}(T)$ do not require any further approximation. Concerning $C_{33}(T)$, close to the PT in the FE phase, the order parameter and the strain were expanded in powers of $T_c - T$ up to the second order. In this approximation, valid in an estimated temperature interval of about 100 K, the expected variation is given in table 4; α and β are functions of the parameters appearing in equations (4)–(8). The resulting values of the adjustable parameters corresponding to the best fits listed in table 5 show similar behaviours for TTP and RTP, but with coupling terms stronger in the first compound. In figure 3 the experimental data deduced from Brillouin scattering can be directly compared with the calculated values. Experimental measurements related to the variation in C_{11} versus temperature show a smoothing of the anomaly near T_c. This effect mainly appears above T_c and is due to fluctuations in the order parameter [20].

Table 4. Temperature dependences of the longitudinal elastic constants deduced from the free energy (4).

Elastic constant	Temperature dependence for the following phases	
	PE ($T > T_c$)	FE ($T < T_c$)
$C_{11}(T)$	$C_{11}^0(T)$	$C_{11}^0(T) - g_1^2/2b$
$C_{22}(T)$	$C_{22}^0(T)$	$C_{22}^0(T)$
$C_{33}(T)$	$C_{33}^0(T)$	$C_{33}^0(T) + h_3\alpha(T_c - T) - h_3^2\beta(T_c - T)^2$

Table 5. Values of the parameters corresponding to the best fits with experimental data using the expressions in table 4.

Compound	Elastic constant	$C_{ii}^0(T_c)$ (GPa)	δ_i (K^{-1})	$g_i^2/2b$ (GPa)	$h_i\alpha$ (GPa)	$h_i^2\beta$ (GPa)
TTP	$C_{11}(T)$	143.3	2.9×10^{-4}	4.2	0	0
TTP	$C_{22}(T)$	138.3	3.8×10^{-4}	0	0	0
TTP	$C_{33}(T)$	148.2	1.2×10^{-4}	0	7.6×10^{-2}	3.5×10^{-4}
RTP	$C_{11}(T)$	139.3	3.9×10^{-4}	2.3	0	0
RTP	$C_{22}(T)$	135.8	4.2×10^{-4}	0	0	0
RTP	$C_{33}(T)$	149.6	1.2×10^{-4}	0	5.4×10^{-2}	1.5×10^{-4}

3.2.2. Quasi-elastic light scattering. The temperature dependences of the $Y(ZZ)\bar{Y}$ recorded Brillouin spectra are shown in figure 4. In addition to the above-mentioned longitudinal lines (L) related to the acoustic phonons, we observe significant quasi-elastic light scattering (QELS). As the temperature is raised, the intensity of the lines increases roughly proportional to the temperature, as expected (in figure 4, all the spectra are normalized to show a constant line intensity). On the other hand, the QELS increases drastically; the ratio of its intensity at 800 K to its value at room temperature is about 20. A similar behaviour for QELS Raman scattering has been reported by several workers [13, 21, 22]. In both compounds the QELS reaches a maximum at about 50 K below T_c and it then decreases abruptly; however, this behaviour is not completely reversible and seems to be at least partially related to sample damage at high temperature. The QELS extends over a broad frequency range in such a way that its frequency dependence cannot be analysed using our Brillouin spectrometer. This QELS originates from the cationic motion, as observed in other superionic conductors [23]. Experimental measurements indicate that the QELS in (ZZ) polarization is significantly larger than in the other polarizations; this agrees with the fact that the ions are confined in a one-dimensional tunnel and consequently move in the c direction only [23].

Besides this broad QELS spectrum we have found a sharper QELS feature near the PT in RTP *but not* in TTP, as shown in figure 4. It consists of wings which appear in a temperature range of a few Kelvin around T_c and is probably related to the coupling of the soft mode to a relaxator; this coupling which has been introduced previously in order to explain the locking of the soft-mode frequency observed through Raman scattering [13, 14] could induce a Brillouin central peak. The involved relaxator could describe Ti displacements within the TiO_6 octahedra, as reported in other FE compounds containing these octahedra [24].

4. Conclusions

The polarized Brillouin spectra of single-crystal KTP, RTP and TTP have been measured at room temperature and all the elastic constants have been deduced. From the variation in

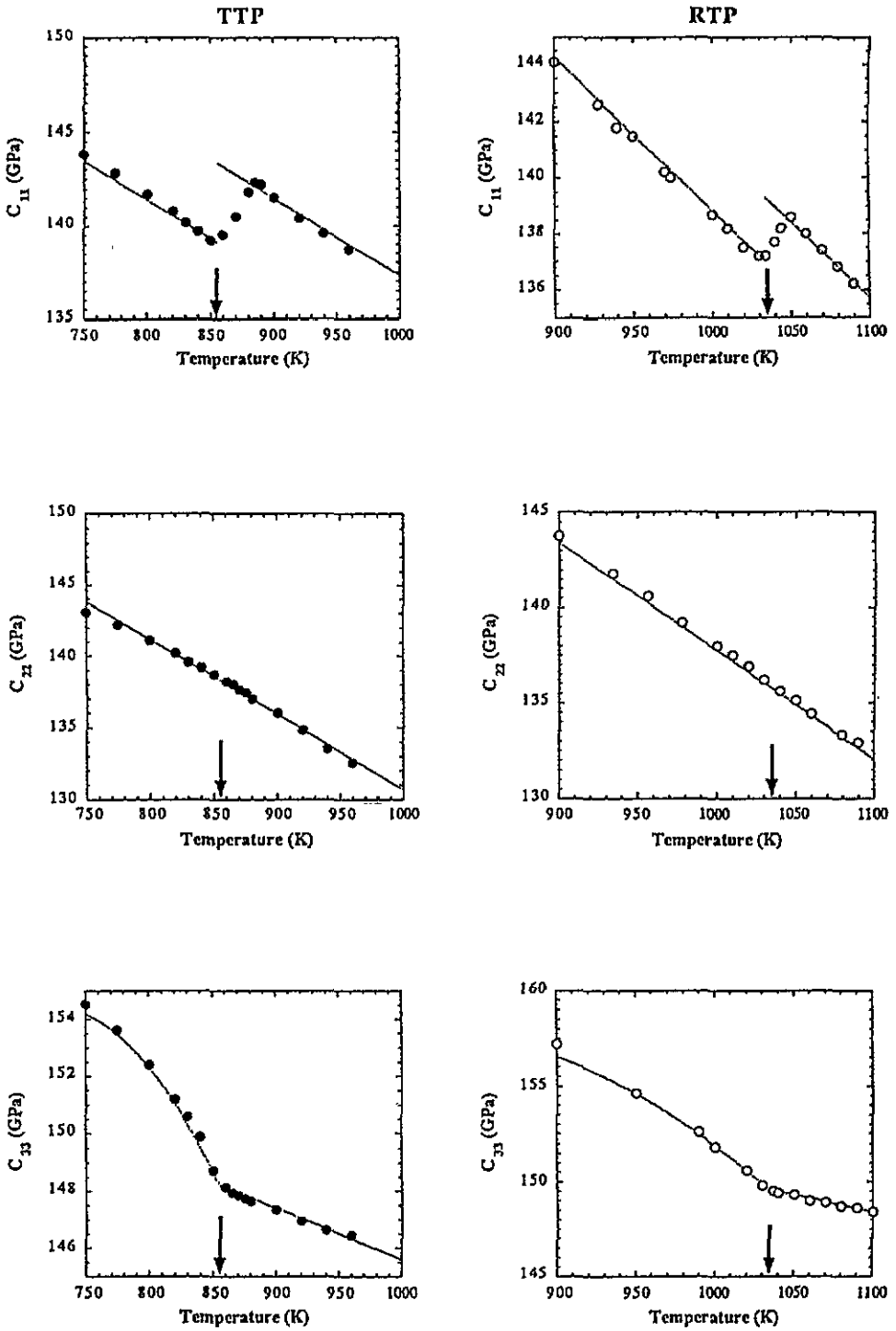

Figure 3. Variations in the longitudinal elastic constants for TTP (●) and RTP (○) versus the temperature. The arrows indicate the transition temperatures. The dotted curves provide the best fits using a Landau model.

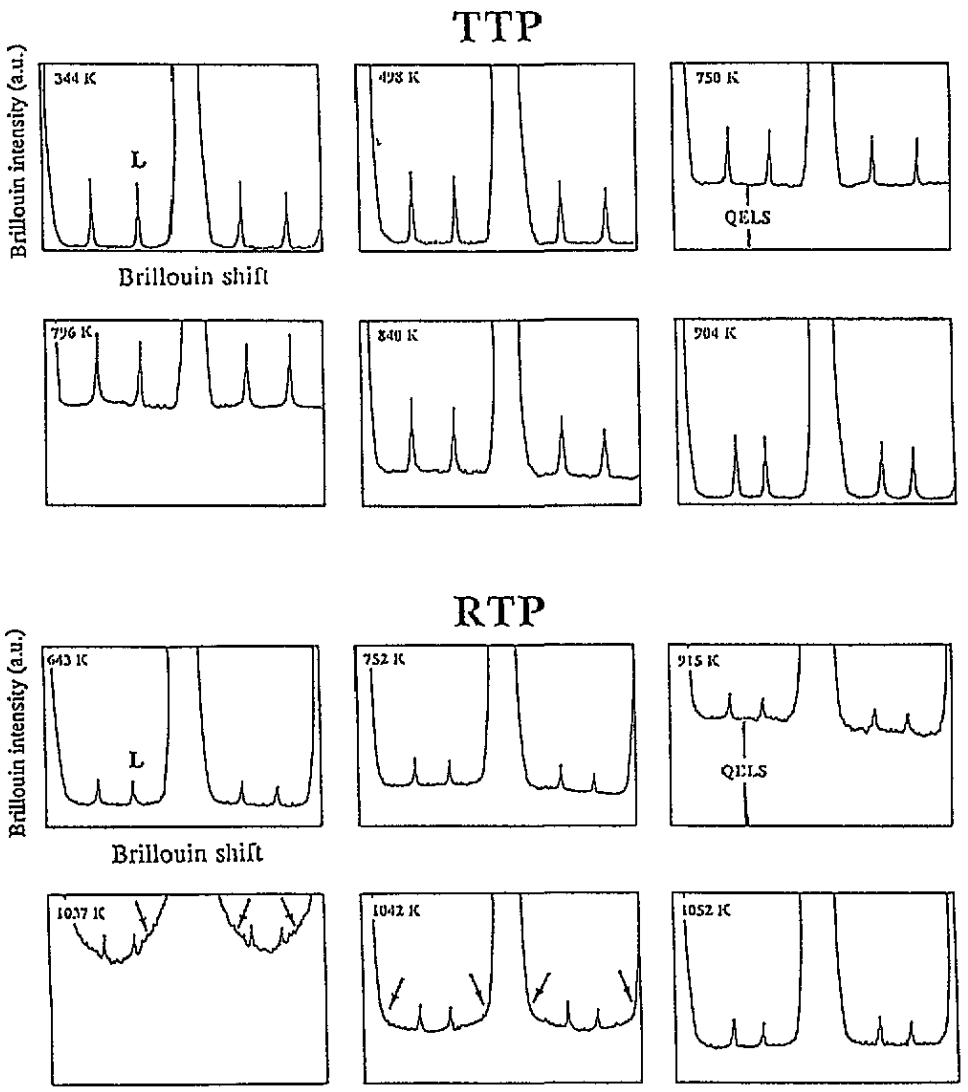

Figure 4. Variation versus temperature of the Brillouin spectra in the $Y(ZZ)\bar{Y}$ geometry for RTP ($T_c \approx 1035$ K) and TTP ($T_c \approx 855$ K). The arrows indicate the central peak contribution for RTP.

the 'longitudinal' elastic constants C_{ii} $(i = 1, 2, 3)$ in the vicinity of the transition, we have shown that the FE–PE transition is most probably of second-order type and that, over a temperature range extending down to about $T_c - 100$, the C_{ii} behaviours can be described using a Landau model; the anomalies observed for TTP and RTP are very similar and agree with the expression for the free energy where the order parameter is quadratically coupled to the strains. On the other hand, we observe significant QELS, related to the quasi-one-dimensional ionic conductivity, as previously observed for other superionic conductors. Finally, for RTP only, a central peak is observed near the transition; it is probably connected to the locking of the soft mode.

Acknowledgments

We thank Dr R V Pisarev of the Ioffe Physico-Technical Institute (Saint Petersburg, Russia) and Dr V I Voronkova of Moscow State University (Physics Department) for supplying us with the crystals studied.

References

[1] Tordjman I, Masse R and Guitel J C 1974 *Z. Kristallogr.* **139** 103
[2] Zumsteg F C, Bierlein J D and Gier T E 1976 *J. Appl. Phys.* **47** 4980
[3] Hansen B F, Protas J and Marnier G 1988 *C. R. Acad. Sci.* (II) **307** 475
[4] Bierlein J D and Arweiler C B 1986 *Appl. Phys. Lett.* **49** 917
[5] Yang H, Gu S J, Xu Z Y, Zhu Y and Li Y Y 1988 *Phys. Rev.* B **37** 1161
[6] Yanovskii V K and Voronkova V I 1980 *Phys. Status Solidi* a **93** 99
[7] Pisarev R V, Markovin P A and Shermatov B N 1989 *Ferroelectrics* **25** 3
[8] Harrison W T A, Gier T E, Stucky G D and Schultz A J 1990 *J. Chem. Soc., Chem. Commun.* p 540
[9] Thomas P A, Glazer A M and Watts B E 1990 *Acta Crystallogr.* B **46** 333
[10] Wang M, Wang J Y, Liu Y G and Wei J Q 1991 *Ferroelectrics* **115** 13
[11] Shaldin Yu V and Poprawski R 1990 *Ferroelectrics* **106** 399
[12] Pisarev R V, Farhi R, Moch P and Voronkova V I 1990 *J. Phys.: Condens. Matter* **2** 7555
[13] Serhane M, Dugautier C, Farhi R, Moch P and Pisarev R V 1991 *Ferroelectrics* **124** 373
[14] Serhane M, Moch P, Farhi R and Pisarev R V 1993 *Proc. 8th Int. Meeting on Ferroelectricity (Gaithersburg, USA)*
[15] Aleksandrov V V, Velichkina T S, Voronkova V I, Koltsova L V, Yakovlev I A and Yanovskii V K 1989 *Solid State Commun.* **69** 877
[16] Landau L and Lifshitz E 1958 *Electrodynamics of Continous Media* (Oxford: Pergamon)
[17] Vacher R and Boyer L 1972 *Phys. Rev.* B **6** 639
[18] Dieulesaint E and Boyer D 1982 *Elastic Waves in Solids* (New York: Wiley)
[19] Rehwald W 1973 *Adv. Phys.* **22** 721
[20] Levanyuk A P 1966 *Sov. Phys.–JETP* **22** 901
[21] Mohamadou B, Kugel G E, Bréhat F, Wyncke B, Marnier G and Simon P 1991 *J. Phys.: Condens. Matter* **3** 9489
[22] Furasawa S, Hayasi H, Ishigame M, Miyamoto A and Sasaki T 1991 *J. Phys. Soc. Japan* **30** 2470
[23] Suemoto T 1990 *Solid State Ion.* **40–41** 250
[24] Maglione M, Böhmer R, Loidl A and Höchli U T 1989 *Phys. Rev.* B **40** 11 441